Contact Dynamics of Internally-Actuated Platforms for the Exploration of Small Solar System Bodies

Robert G. Reid*, Loris Roveda**, Issa A. D. Nesnas*, Marco Pavone***

*Jet Propulsion Laboratory, California Institute of Technology, Pasadena, CA, USA
e-mail: {rgreid, nesnas}@jpl.nasa.gov

**Institute of Industrial Technologies and Automation (ITIA - CNR), Milan, Italy
e-mail: loris.roveda@itia.cnr.it

***Dept. of Aeronautics and Astronautics, Stanford University, Stanford, CA, USA
e-mail: pavone@stanford.edu

Abstract

Directed in-situ science and exploration on the surface of small Solar System bodies requires controlled mobility. In the microgravity environment of small bodies such as asteroids, comets or small moons, the low gravitational and frictional forces at the surface make typical wheeled rovers ineffective. Through a joint collaboration, the Jet Propulsion Laboratory together with Stanford University have been studying microgravity mobility approaches using hopping/tumbling platforms. They have developed an internally-actuated spacecraft/rover hybrid platform, known as "Hedgehog," that uses flywheels and brakes to impart mobility. This paper presents a model of the platform's mobility, analyzing its three main states of motion (pivoting, slipping and hopping) and the contact dynamics between the platform's spikes and various regolith simulants. To experimentally validate the model, an Atwood machine (pulley and counterbalance) was used to emulate microgravity. Experiments were performed with a range of torques on both rigid and granular surfaces while a high-speed camera tracked the platform's motion. Using parameters measured during the experiments, the platform was simulated numerically and its motion compared. Within the limits of the experimental setup, the model is consistent with observations; it indicates the ability to perform controlled forward motions in microgravity on a range of rigid and granular regolith simulants.

1 Introduction

There is increasing interest in exploring small bodies such as asteroids, comets, small moons and near-Earth objects for both science and human missions [1, 2]. One of the biggest challenges associated with this type of target is the microgravity environment that makes surface mobility very challenging. For the smallest potential targets, the gravitational forces can be as low as 10^{-6} g [3].

Small forces normal to the surface and loose or low-friction regolith may make it difficult for wheeled rovers to produce enough traction, thus restricting them to very low velocities [4]. Moreover, the potential exists for wheels to bind on rocky surfaces, whereby a momentary energy build-up could cause the rover to leave the surface in an uncontrolled manner (or exceed escape velocity). Several research groups have considered legged mobility as an alternative to wheels, with anchoring devices at the tip of its appendages [5], however such highly articulated systems are complex, making thermal management challenging.

Other researchers have adopted approaches that use microgravity to their advantage, including hopping or tumbling techniques for surface mobility. In 2005, JAXA

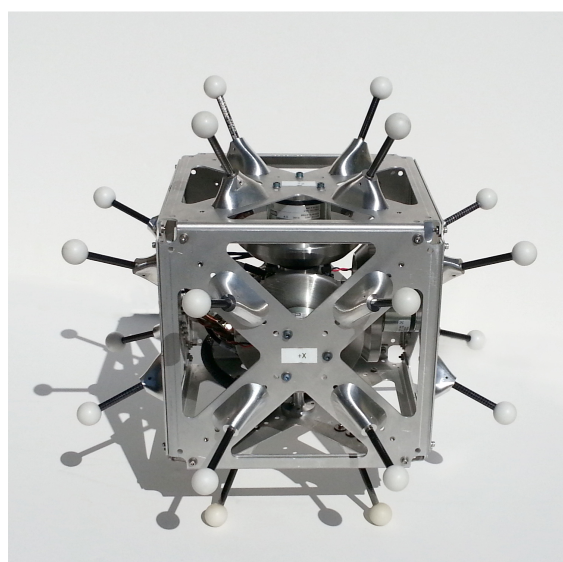

Figure 1. : NASA/JPL Hedgehog platform prototype without avionics, covers or solar panels. The array of protruding spikes provide the contact interface with the surface and protect the platform.

attempted to deploy the MINERVA rover onto the surface of Asteroid (25143) Itokawa from the Hayabusa spacecraft. While the 0.6 kg MINERVA lander didn't reach the surface, JAXA had planned to demonstrate controlled mobility with a single flywheel mounted on a turntable [6]. In late 2014 JAXA is planning to launch Hayabusa 2 to Asteroid (162173) 1999 JU_3 carrying both MINERVA 2 and DLR's MASCOT lander [7]. MASCOT is a 13.5 kg box-shaped lander with an actuated off-center mass. After landing it will use the actuated mass to right itself, and optionally later for uncontrolled mobility.

Our team has been developing a platform to allow controlled mobility in microgravity [8, 9, 10]. The platform uses internal actuation (three mutually-orthogonal flywheels) to generate reaction torques that create mobility. The experimental results in this paper were obtained using the Jet Propulsion Laboratory's prototype, shown in Figure 1. Its external array of spikes protect the platform during motion while providing the primary contact interface with the surface.

In previous work using an earlier prototype [8], Allen et al. showed that such platforms could produce tumbling motions in emulated microgravity (0.024 g). Using an experimental setup similar to the one described in this paper they demonstrated planar 3 degree-of-freedom (DOF) motions that they compared to simulations. Validations were limited to a comparison of the torque levels required to initiate a tumbling/hopping motion. They simulated their prototype by applying the torque profiles measured in their experiments while scaling the profiles to best correlate the results (mean scale factor was 106%). In our experiments we collect significantly more data, including the platform's 6 DOF pose at 120 Hz, and directly compared simulated and experimental trajectories. Our comparisons also include an analysis of the sensitivities to surface friction coefficients.

Small bodies may have complex and varying morphologies: from rocky or icy surfaces to fine granular regolith. Surface observations of the Asteroid Itokawa are currently the highest quality observations of complex rocky and granular morphologies [11]. The ability of a platform to move over such surfaces depends on the magnitude of the reaction forces between a platform's contacts and the surface. Further, the ability to direct the motion depends on having sufficient friction, hence reaction force to accelerate across the surface.

Koenig et al. analyzed both linear and angular actuation of platforms using a Coulomb friction model for surface contact [10]. They provide an analysis of forces and the resulting constraints on motion for a platform that either pivots over its contact points, or slips, and describe a set of viable hopping angles. In this work, we use numerical simulations and high-speed video of experiments to show the dynamic nature of transitions between pivoting and slipping motions, including the possibility of controlling the hopping angle within the viable range described by Koenig et al. We increase the fidelity of the contact model, and approximate compliance in both the surface and the platform, by adding a spring-damper component that acts normal to the surface [12]. We note that small bodies are unlikely to be smooth and homogeneous, however the model may be sufficient to analyze mobility on rigid parts of their surface.

For complex or non-rigid surfaces including granular regolith, pebbles or ice, realistic contact models are harder to derive and validate. In microgravity environments, the forces interacting with the regolith are likely to be much stronger than the local surface gravity field [13]. The main factors affecting contact dynamics with granular regolith are i) the compressive strength of the regolith, ii) the dynamic drag term resulting from the transfer of momentum from the platform to the ground (proportional to the granular media density and the square of velocity of the contact) and iii) the sliding friction at the contact interface. DLR developed a "soil" contact model for MASCOT, based on planetary rover wheel-soil interactions [7]. They used terramechanics theory to evaluate the contact dynamics between MASCOT's rectangular faces and regolith in microgravity. Contact models for granular regolith remain an open research question.

High-level mission architectures to small Solar System bodies have been explored. One such architecture includes a "mother" spacecraft with one or more deployable platforms [9, 14]. Aside from mobility, there are various other challenges deploying platforms on small bodies including soft-landing on the surface. Tardivel and Scheeres simulate trajectories for approaching small bodies [15] and, using high-level stochastic models, they consider a passive "pod" bouncing around on the surface for many hours until coming to rest.

The closest terrestrial equivalent to the Hedgehog prototype is "Cubli", a $15 \times 15 \times 15$ cm cube with 3 orthogonal flywheels [16]. To operate in the Earth's gravity, Cubli requires orders of magnitude more torque, which it creates using a braking mechanism. Gajamohan et al. have demonstrated Cubli hopping onto one corner and balancing in an inverted pendulum configuration. Using precise torque control they have demonstrated a sequence of controlled tumbles and maneuvers while balancing.

In the next section, we give an overview of our platform design principles including our current Hedgehog prototype. Section 3 presents our model for the platform's dynamics including its three main states of motion (pivoting, slipping and hopping) and the regolith contact model during these states. The experimental setup used to validate our model is presented in Section 4, with various results and analysis in Section 5 and Section 6.

2 Platform Description

The spacecraft/rover hybrid we describe here is a mobility platform that uses internal flywheels to produce tumbling or hopping motions. It is supported and protected from the surface by an array of external spikes. We are considering designs that are about ≈ 0.5 m in diameter and ≈ 5 kg in mass. The design is scalable depending on payload accommodations [9]. Our current Hedgehog prototype, shown in Figure 1, has 24 external spikes forming a *rhombicuboctahedron* and providing an octagonal cross-section of 0.4 m in diameter. The platform is normally supported by four spikes forming a square base and occasionally supported by three spikes forming a less stable triangular support. We expect the final mass with covers and solar panels to be around 10 kg.

The platform uses no external propulsion. Instead, it is actuated by three mutually-orthogonal flywheels enclosed in the body. Benefits of this design include simpler environmental sealing and thermal management [9]. Using a linear combination of torques, the three flywheel motors can produce reaction torques at the surface in any orientation without additional moving parts. Regarding mobility, the design is expected to be safer and more capable than wheeled rovers. The internal torques can produce momentarily large reaction forces at the surface resulting in increased acceleration across the surface. By dynamically controlling the flywheel torques, the platform can perform motions such as small tumbles across the surface or large ballistic hops.

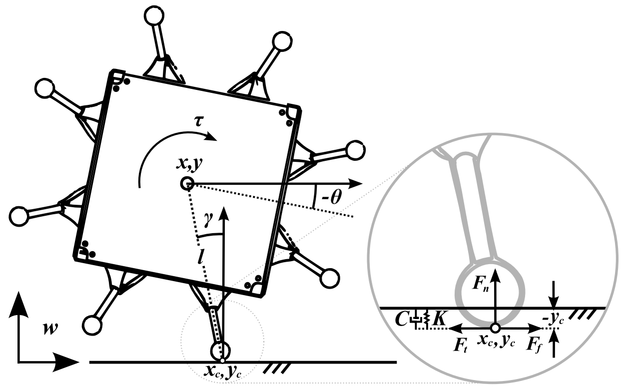

Figure 3. : Platform and contact schematic.

Parameter	Definition
$q = (x, y, \theta)$	Platform pose
m_{hh}	Platform mass
J_{hh}	Platform inertia matrix
l	Spike length from the center to the pivot
τ	Torque applied by flywheel
μ_s, μ_d	Static and dynamic friction coefficients
K	Surface stiffness
C	Surface damping
g	Gravity at surface (m/s^2)

Table 1. : Platform and environment parameters.

3 Dynamic Analysis

This section derives a dynamic model for the platform with equations of motion provided for its three main states: pivoting, slipping and hopping. We define a contact model for the pivoting and slipping states when the platform's spikes contact the regolith surface. Figure 3 provides a schematic of the dynamic model, while Table 1 lists the parameters used throughout this paper.

To simplify the analysis, the platform's mass distribution is assumed to be uniform with its center of mass coinciding with its geometric center. By operating only a single flywheel, the platform's motion is restricted to a plane. It's initial pose, parameterized by $q = (x, y, \theta)$, is $\left(0, l\cos\frac{\pi}{8}, 0\right)$ at rest. The regolith surface is assumed to be flat and homogeneous, while contact interfaces with the spikes are modeled as uniform points. The contact equations comprise of a spring-damper component [12] that is normal to the surface, and a Coulomb friction component that acts tangential to the surface.

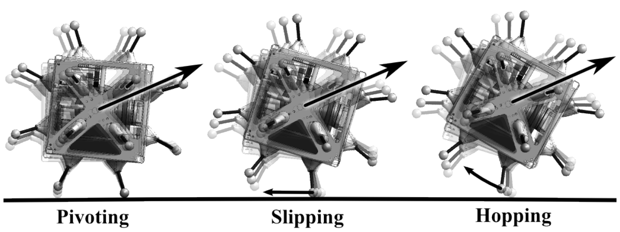

Figure 2. : Three main states of motion.

Figure 2 illustrates a typical hopping motion. The torque τ, applied to the platform at rest, causes it to pivot over its two leading spikes until the horizontal component of the contact force becomes greater than the static friction force . A period of slipping motion typically follows where the platform rotates forward and the same two spikes are dragged backwards in contact with the surface. Given sufficient energy, the platform will then leave the surface, hopping forwards in a ballistic trajectory. The profile of the torque $\tau(t)$ determines whether a tumble or a hop is executed. In this analysis, a constant torque is applied for the duration of any contact with the surface.

Transitions between states are determined by the presence of interactions (contacts) between spikes and the surface. If the tip of a spike intersects the surface, the reaction force on the spike at the contact consists of a normal component F_n and a tangential component F_t. The Coulomb model for static friction provides the upper bound on F_t to maintain a pivoting motion: $F_t < \mu_s F_n$. Once the platform transitions to a slipping motion, the dynamic friction coefficient places a lower bound on F_t to keep slipping: $F_t > \mu_d F_n$. If no spikes are intersecting the surface, the platform is in a ballistic (hopping) trajectory.

We model the platform with a Lagrangian approach where $q = (x, y, \theta)$ is a vector describing the platform's pose:

$$\frac{d}{dt}\frac{\partial T}{\partial \dot{q}} - \frac{\partial T}{\partial q} + \frac{\partial D}{\partial \dot{q}} + \frac{\partial V}{\partial q} = \frac{\partial \delta L}{\partial \delta q} \tag{1}$$

T is the kinetic energy, D is the dissipated energy, V is the potential energy, L is the virtual work of external forces and $\frac{\partial \delta L}{\partial \delta q}$ is the Lagrangian component of the external forces. We derive each of these terms in the following sections.

3.1 Contact Dynamics

Contact points are defined during motions where one or more spikes penetrate the surface. Our Hedgehog platform has an octagonal cross-section, where eight spikes of length l are separated by 45°. The spikes are rigidly connected to the platform, and therefore rotate with θ. The contact angle from vertical, γ, for each spike, is:

$$\gamma(\theta, n) = \theta + \frac{\pi}{8} + \frac{\pi}{4}n, \qquad n = 1, 2 \ldots 8 \tag{2}$$

The inset in Figure 3 shows a spike contact point, (x_c, y_c). The penetration depth for the spike, y_c, is a function of the platform's height, y, and spike rotation, γ:

$$y_c = y - l\cos\gamma \tag{3}$$

Similarly the horizontal position of the contact, x_c, is:

$$x_c = x + l\sin\gamma \tag{4}$$

For a spike penetrating y_c into the elastic surface K, the stored potential energy is defined:

$$V_c = \frac{1}{2}Ky_c^2 \ \forall \ y_c < 0 \tag{5}$$

The dissipative energy is defined by a damping term, proportional to the square of the spike's penetration velocity:

$$D_c = \frac{1}{2}C\dot{y_c}^2 \ \forall \ \dot{y}_c < 0 \tag{6}$$

Here the damping term is only applied when $\dot{y}_c < 0$, as the spike is actively penetrating into the surface and dissipating energy. During slipping motions each contact produces the friction force $F_f = -sign(\dot{x}_c)\mu_d F_n$. This creates a virtual work term:

$$L_c = F_f x_c \tag{7}$$

3.2 Slipping and Hopping Dynamics

Hopping is the simplest motion state since no surface contact exists ($y_c > 0$). During hopping, the platform undergoes unrestrained 3 DOF ballistic motion, $q = (x, y, \theta)$. During slipping, the platform's pose is constrained such that contact points slide along the surface, however it still undergoes 3 DOF motion. Thus the same dynamic equations are used for both slipping and hopping. For hopping motions the contact-related terms V_c, D_c and L_c are zero. The kinetic energy of the platform is defined:

$$T = \frac{1}{2}m_{hh}\left(\dot{x}^2 + \dot{y}^2\right) + \frac{1}{2}J_{hh}\dot{\theta}^2 \tag{8}$$

The potential energy in the system is defined by a gravitational term and the term due to contact V_c (if any):

$$V = m_{hh}gy + V_c \tag{9}$$

If a contact exists, the dissipative energy $D = D_c$ is given in equation 6. The virtual work L that results from applying a torque τ on the flywheels is given by $\tau\theta$, and while slipping, the work done against friction, L_c, from equation 7:

$$L = \tau\theta + L_c \tag{10}$$

Using equations 2, 3 and 4, the contact-related terms V_c, D_c and L_c can be rearranged in terms of x, y and θ. Applying the Lagrangian approach, the contact dynamics are:

$$\begin{aligned}
m_{hh}\ddot{x} &= F_f && (11)\\
m_{hh}\ddot{y} + m_{hh}g + K\left[y - l\cos(\theta)\right] & && \\
+C\left[\dot{y} + l\sin(\theta)\dot{\theta}\right] &= 0 && (12)\\
J_{hh}\ddot{\theta} + l\sin(\theta)\left[K\left(y - l\cos(\theta)\right)\right. & && \\
\left.+C\left(\dot{y} + l\sin(\theta)\dot{\theta}\right)\right] &= \tau - F_f\cos(\theta) && (13)
\end{aligned}$$

3.3 Pivoting Dynamics

During a pivoting motion, the platform's pose $q = (x, y, \theta)$ is constrained to rotate on an arc with a radius l centered on the contact point. To simplify calculations, the constrained pose is parameterized using 2 DOF: the platform rotation, θ, and the vertical penetration of the spike at the contact point, $y_c \leq 0$, given in equation 3.

The kinetic, T, and potential, V, terms are given in equation 8 and 9. The dissipative energy in the contact $D = D_c$ is given in equation 6. Differentiating and substituting equations 2 and 3 into T, V and D results in functions of y_c, $\dot{y_c}$, θ, and $\dot{\theta}$. The virtual work L is given by the torque, τ, that the flywheel applies during the pivoting motion:

$$L = \tau\theta \tag{14}$$

By applying the Lagrangian approach, the 2DOF pivoting contact dynamics are:

$$\begin{aligned} m_{hh}\left[\ddot{y_c} + l\sin(\theta)\ddot{\theta} + l\cos(\theta)\dot{\theta}^2\right] & & \\ +C\dot{y_c} + Ky_c + m_{hh}g &= 0 & (15) \\ \left(m_{hh}l^2 + J_{hh}\right)\ddot{\theta} + m_{hh}l\sin(\theta)\ddot{y_c} & & \\ +m_{hh}gl\sin(\theta) &= \tau & (16) \end{aligned}$$

4 Experimental Setup and Procedure

Experiments were performed to validate the analytical model presented in Section 3. The setup is shown in Figure 4. An Atwood machine was configured as a gravity offloading test bed. The platform was secured through its center of mass by a shaft and a pair of bearings so that it could rotate freely. Two high-tensile steel wires were connected to the bearings, looped over two pulleys and connected to a counterbalance suspended on the other side. The large diameter light-weight pulleys were free to rotate around low-friction bearings. With the counterbalance offsetting most of the platform's mass, experiments were performed on a range of regolith simulants.

Using the test bed, we were able to simulate gravity levels on the order of 10^{-2} g. However, this type of platform (described in Section 2) targets surface gravity levels several orders smaller (from $\approx 10^{-4}$ g on Mars' moon Phobos down to 10^{-6} g on small asteroids). The flywheel motors in the prototype produce a maximum of 0.22 Nm torque, which can only produce tumbles in the test bed. To apply larger torques and analyze hopping, the prototype includes electromechanical brakes that decelerated the flywheels to produce ≈ 6.0 Nm torque.

The total mass of the prototype was 5.3 kg, and with the matching counterbalance mass, the additional inertia limited mobility further. The additional mass also created artificial stresses in the chassis impacting braking performance. To reduce the mass and corresponding chassis stress, only one of the three flywheel and brake assemblies were installed for the experiments. The motor controllers were installed in the prototype, however the avionics were off-board to minimize weight. A light-weight 3-wire umbilical was used to communicate with the platform, supported to prevent disruption to the platform's dynamics during motion. Power was supplied from on-board lithium polymer batteries.

The configuration allowed for two translational and one rotational degrees of freedom, providing about 40 mm of free motion in simulated microgravity before tangential forces from the pendulum distorted the trajectory. This provided enough range of motion to allow the initial trajectory to be characterized. Data recorded during experiments included the velocity of the flywheel at 600 Hz and the platform's rotation rates and accelerations with an inertial measuring unit (IMU) at 100 Hz. The platform's

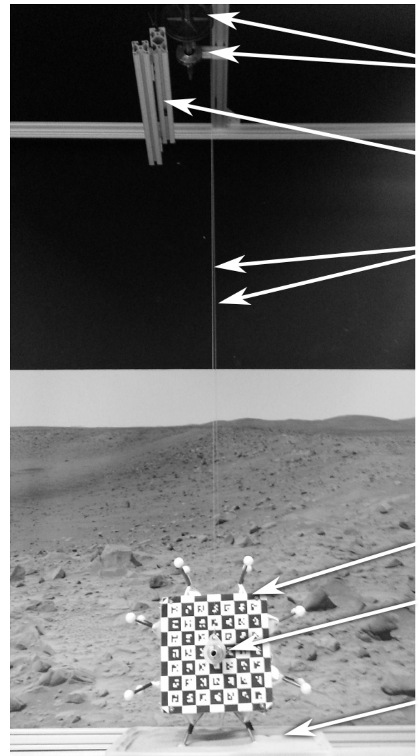

Figure 4. : Gravity offloading test bed: an Atwood machine offsets the weight of the Hedgehog platform allowing different gravity levels to be simulated.

pose was tracked in 6 DOF at 120 Hz using an external high-speed video camera and visual fiducial markers [17]. The tracking quality was monitored throughout the experiments and millimeter pose accuracy was maintained. The video was also used to identify motion state transitions.

Experiments were performed at two simulated gravity levels (0.015 g and 0.0085 g). For each gravity, level three torques (0.125 Nm, 0.22 Nm and 6.0 Nm) were evaluated on four different surfaces. To simulate rocky and icy regolith, a limestone brick and steel plate were used. To simulate granular regolith, beds of fine sand and JSC-1A Lunar simulant [18] were used.

The experimental procedure included preparations such as aligning the pulleys to minimize friction, and then allowing the platform to come to rest on the surface, supported by four spikes. For the granular regolith experiments the media was "fluffed" and leveled before each test. Granular media properties were measured with a small conical penetrometer.

4.1 Gravity Offloading Setup Dynamics

During dynamic motions the gravity offloading setup causes the counterbalance to move in the vertical (y) direction, while the platform's center of mass moves in the x, y plane. The rigid coupling between the masses, and the platform's pendulum-like motion creates a potentially complex dynamic system. While the Lagrangian components are tractable, by only considering the first 40 mm of the platform's motion, the dynamics are simplified. With the offloading pulleys 2.2 m above the platform, the arc angle $\frac{40}{2200} \approx 1.0°$ is small enough to use small-angle approximations.

To compare simulated and experimental results we model the counterbalance mass, m_b, by adding two terms to the Lagrangian equations. The velocity of the counterbalance, $\dot{y}_b$, is approximated by:

$$\dot{y}_b \cong -\dot{y} \tag{17}$$

The kinetic and potential energy terms for the counterbalance are hence:

$$\begin{aligned} T_b &= \frac{1}{2} m_b \dot{y}_b^2 \\ V_b &= m_b y_b g \end{aligned} \tag{18}$$

4.2 Numerical Simulations

We performed numerical simulations using the platform's analytical model, derived in Section 3, and the offloading setup model from Subsection 4.1. The discrete-time simulation was programmed in Matlab with a fixed 1 ms time-step and parameters that were measured experimentally. Simulated trajectories appeared most sensitive to the static and dynamic friction coefficients, however we

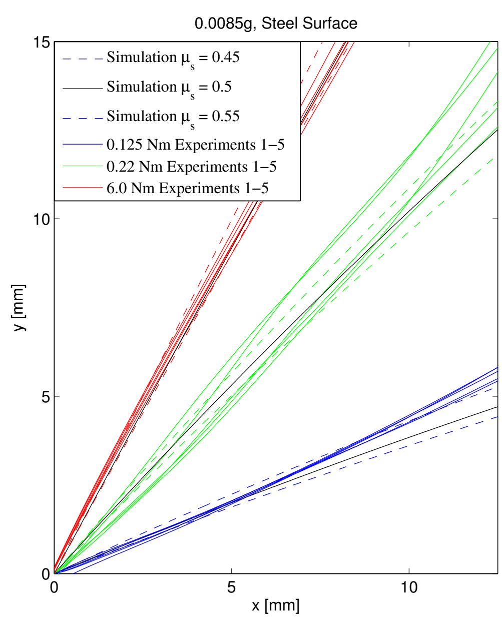

Figure 5. : Initial platform trajectories. Both experimental and simulated trajectories are shown in simulated 0.0085 g. As the torque increases (0.125 Nm, 0.22 Nm and 6.0 Nm) the trajectory angle increases also. Sensitivity to the static friction coefficients ($\mu_s = 0.25$) is indicated by the bounding ±10% simulations.

note these were the hardest to measure accurately. In each of the simulations we evaluated this sensitivity by simulating ±10% of the friction coefficients. The dynamic friction coefficients were fixed to half of the static value: $\mu_d = \mu_s/2$.

5 Results

Figure 5 shows the platform's initial trajectories while completing motions on the steel surface ($\mu_s = 0.25$) with a simulated gravity level of 0.0085 g. Experimental and simulated trajectories match well. Differences begin to appear in some trajectories where the prototype appears to push away from the surface faster. This may be caused by vibrations through the platform as the flywheels accelerate/decelerate. Spike vibrations at the contact point cause it to "skip" over the surface and greatly reduce the dynamic friction coefficient. Pendulum-like effects, due to the offloading setup, are observed over larger trajectories (> 50 mm). As the applied torque increases the trajectory angle increases also, to a maximum of about 60 degrees.

To further validate our model the state transitions between pivoting, slipping and hopping are plotted in Figure 6. Even for a short tumble in 0.0085 g the simulation predicts the platform will break contact with the ground and perform a brief hop. Analyzing the high-speed video confirms this in 5 of 6 cases. Similarly the majority of the transition angles in the experimental occur within 5 degrees of the simulated angles. Figure 6 includes markers where the pendulum effect begins to affect motion in the experiments. State transitions after these markers are not expected to match well. The 6.0 Nm torque simulations show a harmless artifact in the transition to hopping that is not observed in the experiments.

To demonstrate that the platform can produce forward motions on a variety of surfaces, the initial trajectory angles, maximum linear and angular velocities were plotted in Figure 8. Most of the low-torque experiments (0.125 Nm and 0.22 Nm) produced slow, tumbling motions that can be identified by the ≈ 22.5 degree initial trajectory angle. Five experiments exceed this angle, indicating hopping trajectories. Four of these experiments used the higher torque from the brakes (6.0 Nm), for which Figure 6 confirms that the platform begins to slip almost immediately, which is consistent with the predictions in [10] for high-energy hops. Figure 7 extrapolates the initial hopping trajectory from these experiments, suggesting what the unrestrained hopping trajectories could have looked like. Simulated trajectories agree well with the extrapolated experimental data. Four experiments in Figure 8 have negative trajectory angles, corresponding to the brake being used on granular simulants. In each of these experiments the platform made good forward progress, however sank into the simulant slightly due to initial conditions.

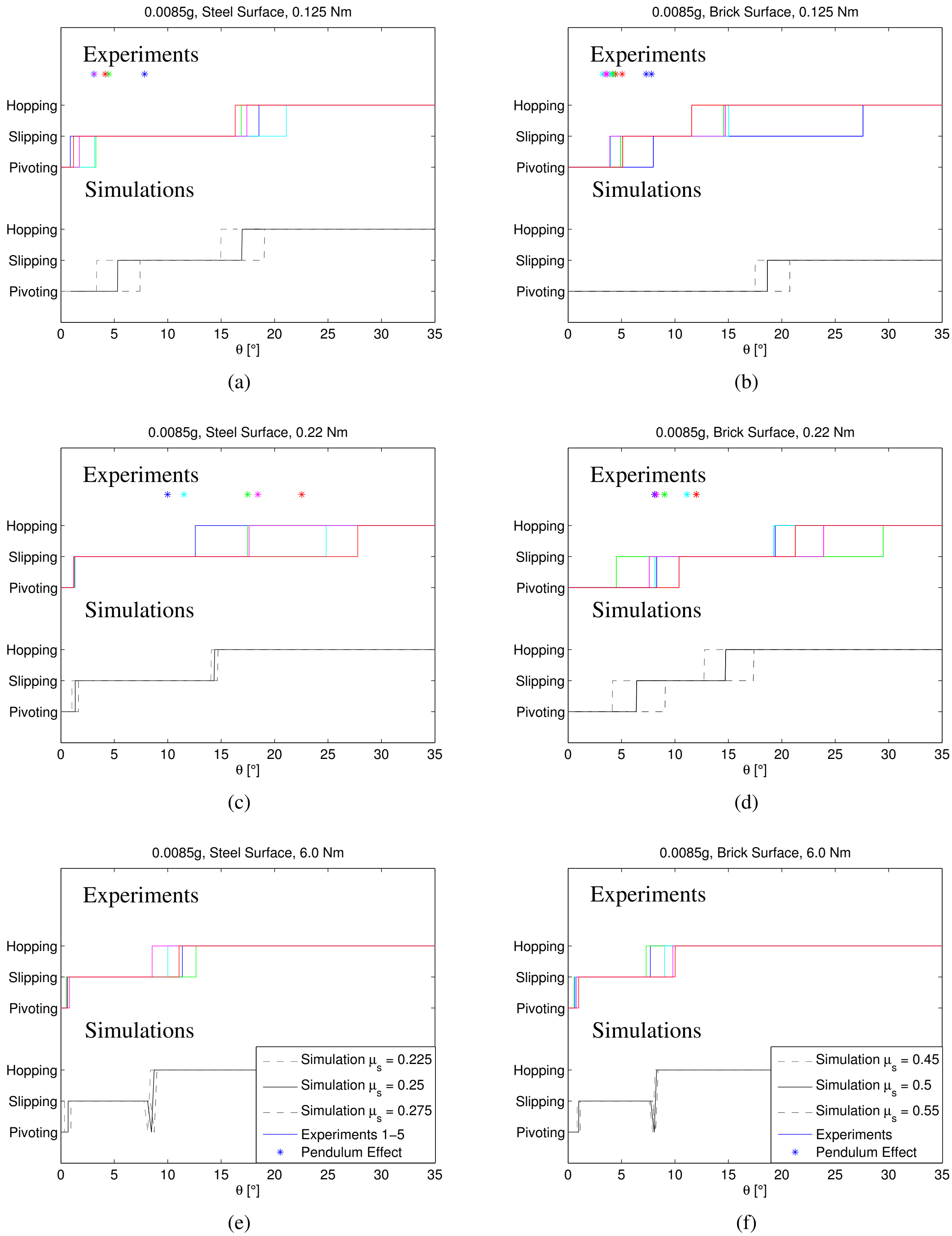

Figure 6. : Motion state transitions during a tumble (a, b, c and d) and hop (e and f) with gravity level 0.0085 g. Left (a, c and e) the steel surface with $\mu_s = 0.25$ and right (b, d and f) the brick surface with $\mu_s = 0.50$. The torques applied to produce the hops/tumbles are (a and b) 0.125 Nm, (c and d) 0.22 Nm, (e and f) 6.0 Nm. Sensitivity to the static friction coefficients are indicated by the bounding ±10% simulations.

6 Conclusions

We have presented an analytical model for the Hedgehog platform, considering its three main states of motion (pivoting, slipping and hopping) and the contact dynamics between the platform's spikes and rigid surfaces. Experiments were performed at two simulated microgravity levels (0.0085 g and 0.015 g), and with a range of torques (0.125 Nm, 0.22 Nm and 6.0 Nm). Numerical simulations using parameters measured in the experiments were compared and show close correlation with the experimental observations, within the limits of the experimental setup. Experiments on four surfaces (brick, steel, sand and JSC-1A) indicate that the platform can perform forward motions in simulated microgravity. The correlation observed between torque and trajectory angles suggests that dynamically controlling the torque may enable hopping angles to be controlled.

One source of discrepancies between the analytical model and experiments results from vibrations induced by the flywheels. These vibrations disrupt the Coulomb friction at the spike's contact, effectively decreasing the static friction coefficients. Modeling the spike's vibration modes may resolve part of this discrepancy. Small irregularities in the surfaces, particularly the brick surface, further amplify this effect, however they are difficult to model. Errors in parameter measurements, slightly off-center platform mass (non-uniform mass distribution) and the assumption of a point contact (l varies with angle γ for a spherical spike) may contribute to small discrepancies that were observed. Experiments with the granular simulants indicate the platform can make forward progress on lightly-packed regolith, however, multiple tumbles are needed to provide more realistic initial conditions for successive tumbles and to confirm that the platform will not

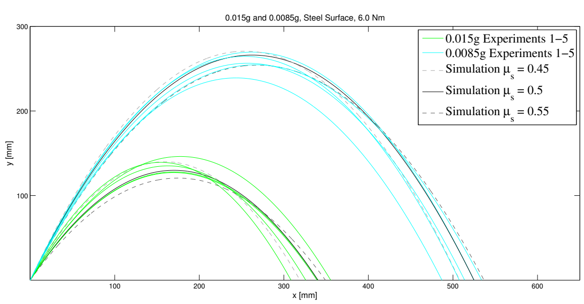

(a)

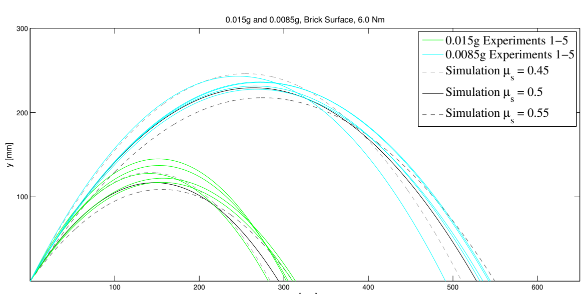

(b)

Figure 7. : Extrapolated hopping trajectories on (a) the steel surface and (b) the brick surface at both gravity levels (0.015 g and 0.0085 g). The parabolic hops have been extrapolated from the trajectory angles and velocities measured in the experiments. These hops were not possible due to the experimental setup.

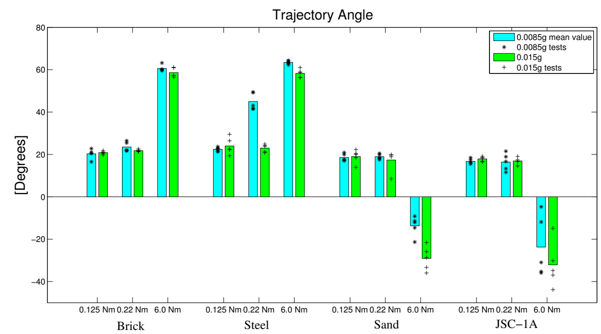

(a)

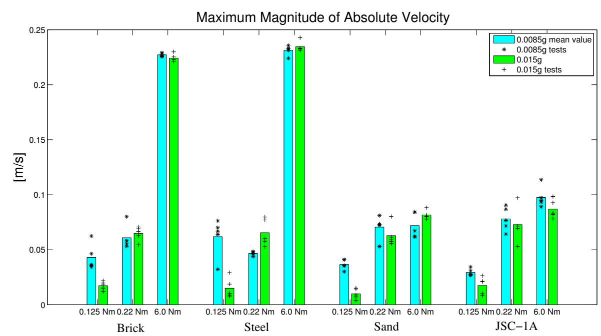

(b)

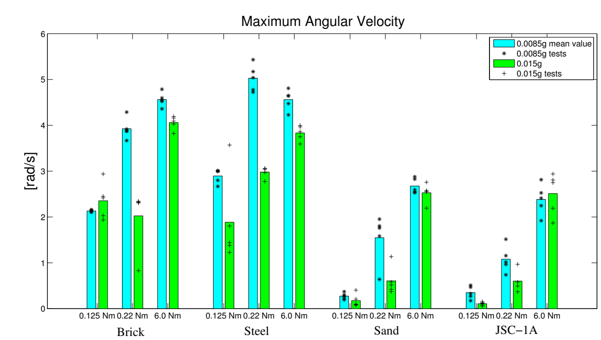

(c)

Figure 8. : (a) The initial platform trajectory angle, (b) maximum linear velocity magnitude and (c) angular velocity. This figure captures all experiments performed: two gravity levels (0.015 g and 0.0085 g) with three torques (0.125 Nm, 0.22 Nm and 6.0 Nm) evaluated on four different surfaces (brick, steel, sand and JSC-1A).

continue to sink. This is not possible with the current gravity offloading setup.

Future work includes addressing deficiencies in the gravity offloading setup. Our collaborators at Stanford are currently developing an actuated 6 DOF gantry, where the vertical axis uses a voice-coil to increase the fidelity of gravity offloading. Actively "fluffing" granular simulants with air fluidization may allow contact dynamics to be explored in microgravity, however designing comprehensive microgravity mobility experiments remains a challenge. Another avenue for future work is to simulate both the platform and granular media with multi-body discrete element methods, however computational requirements and model validation remains an open research problem. In the near-term our team is planning to further validate the Hedgehog platform's mobility in a campaign of parabolic flights on a zero-g aircraft.

Acknowledgments

We would like to thank Kun ho Kim for his inital analysis of the motion states and their transitions. This research was carried out at the Jet Propulsion Laboratory, California Institute of Technology, under a Contract with the National Aeronautics and Space Administration.

References

[1] T. Yoshimitsu, T. Kubota, S. Aakabane, I. Nakatani, T. Adachi, H. Saito, and Y. Kunii, "Autonomous navigation and observation on asteroid surface by hopping rover MINERVA," in *i-SAIRAS*, 2001.

[2] A. F. Cheng, "Near Earth asteroid rendezvous: mission summary," *Asteroids III*, pp. 351–366, 2002.

[3] D. Scheeres, S. Broschart, S. Ostro, and L. Benner, "The dynamical environment about Asteroid 25143 Itokawa: target of the Hayabusa Mission," in *AIAA/AAS Astrodynamics Specialist Conference and Exhibit*, 2004.

[4] B. H. Wilcox and R. M. Jones, "The MUSES-CN Nanorover mission and related technology," in *IEEE Aerospace Conference Proceedings*, vol. 7, 2000.

[5] B. H. Wilcox *et al.*, "ATHLETE: A cargo handling and manipulation robot for the moon," *Journal of Field Robotics*, vol. 24, no. 5, pp. 421–434, 2007.

[6] T. Yoshimitsu, T. Kubota, and I. Nakatani, "MINERVA rover which became a small artificial solar satellite," *AIAA/USU Conf. on Small Satellites*, 2006.

[7] C. Dietze, F. Herrmann, S. Kuß, C. Lange, M. Scharringhausen, L. Witte, T. van Zoest, and H. Yano, "Landing and mobility concept for the small asteroid lander MASCOT on asteroid 1999 JU3," in *61st International Astronautical Congress*, 2010.

[8] R. Allen, M. Pavone, C. McQuin, I. A. Nesnas, J. Castillo, T.-N. Nguyen, and J. Hoffman, "Internally-actuated rovers for all-access surface mobility: Theory and experimentation," in *Proc. IEEE Conf. on Robotics and Automation*, 2012.

[9] M. Pavone, J. C. Castillo-Rogez, J. A. Hoffman, I. A. D. Nesnas, and N. J. Strange, "Spacecraft/Rover hybrids for the exploration of small solar system bodies," in *Aerospace Conference, 2013 IEEE*, 2013.

[10] A. W. Koenig, M. Pavone, J. C. Castillo-Rogez, and I. A. Nesnas, "A Dynamical Characterization of Internally-Actuated Microgravity Mobility Systems," in *IEEE Conf. on Robotics and Automation*, 2014.

[11] H. Yano, T. Kubota, H. Miyamoto, T. Okada, D. Scheeres, Y. Takagi, K. Yoshida, M. Abe, S. Abe, O. Barnouin-Jha, *et al.*, "Touchdown of the Hayabusa spacecraft at the Muses Sea on Itokawa," *Science*, vol. 312, no. 5778, 2006.

[12] G. Gilardi and I. Sharf, "Literature survey of contact dynamics modelling," *Mechanism and machine theory*, vol. 37, no. 10, 2002.

[13] B. Quadrelli, H. Mazhar, and D. Negrut, "Modeling and Simulation of Anchoring Processes for Small Body Exploration," in *AIAA SPACE 2012 Conference & Exposition*, 2012.

[14] J. Castillo-Rogez, M. Pavone, I. Nesnas, and J. Hoffman, "Expected science return of spatially-extended in-situ exploration at small solar system bodies," in *2012 IEEE Aerospace Conference*, 2012.

[15] S. Tardivel and D. J. Scheeres, "Ballistic deployment of science packages on binary asteroids," *Journal of Guidance, Control, and Dynamics*, vol. 36, 2013.

[16] M. Gajamohan, M. Muehlebach, T. Widmer, and R. D'Andrea, "The Cubli: A reaction wheel based 3D inverted pendulum," in *European Control Conference (ECC)*, vol. 2, 2013.

[17] B. Atcheson, F. Heide, and W. Heidrich, "CALTag: High Precision Fiducial Markers for Camera Calibration," in 15$^{\text{th}}$ *International Workshop on Vision, Modeling and Visualization*, 2010.

[18] X. Zeng, C. He, H. Oravec, A. Wilkinson, J. Agui, and V. Asnani, "Geotechnical properties of JSC-1A lunar soil simulant," *Journal of Aerospace Engineering*, vol. 23, no. 2, 2010.